Virology 444 (2013) 225–232

Contents lists available at ScienceDirect

Virology

journal homepage: www.elsevier.com/locate/yviro

Identification of two ATR-dependent phosphorylation sites on coronavirus nucleocapsid protein with nonessential functions in viral replication and infectivity in cultured cells

Shouguo Fang [a,b,1], Linghui Xu [b,1], Mei Huang [b,1], Frank Qisheng Li [b], D.X. Liu [b,*]

[a] Agricultural School, Yangtze University, 266 Jingmilu, Jingzhou City, Hubei Province 434025, China
[b] School of Biological Sciences, Nanyang Technological University, 60 Nanyang Drive, Singapore 637551, Singapore

ARTICLE INFO

Article history:
Received 12 April 2013
Returned to author for revisions
27 April 2013
Accepted 10 June 2013
Available online 9 July 2013

Keywords:
Coronavirus
N protein
Phosphorylation
ATR/Chk1 pathway
Replication

ABSTRACT

Coronavirus encodes an extensively phosphorylated and highly basic nucleocapsid (N) protein. Previous studies have identified Ser190, Ser192, Thr378 and Ser379 as the phosphorylation sites for coronavirus infectious bronchitis virus (IBV) N protein. In this study, we show that phosphorylation at Thr378 and Ser379 sites is dependent on the ataxia-telangiectasia mutated (ATM) and Rad3-related (ATR), a kinase activated during IBV replication. Introduction of Ala substitutions at these two sites individually, in combination of the two and together with other two sites (Ser190 and Ser192) into an infectious IBV clone did not affect recovery of the recombinant viruses containing the mutations. A mutant virus (rIBV-Nm4) carrying the four Ala substitutions grew at a similar, if not better, growth rate as wild type virus. This study reveals a cellular kinase responsible for phosphorylation of a coronavirus N protein at two positions and the functional consequence of this modification on coronavirus replication.

Introduction

Coronavirus is an enveloped virus with a single strand, positive-sense RNA genome of 27–30 kb length. In cells infected with coronavirus, a 3′-coterminal nested set of 6–9 mRNAs species, including the genome-length mRNA (mRNA1) and 5–8 subgenomic mRNA species (mRNA2–9), is expressed. The genome-length mRNA1 encodes two overlapping replicase proteins in the form of polyproteins 1a and 1ab, which are processed by virus-encoded proteinases into at least 15 putative nonstructural proteins (NSP1–NSP16) (Fang et al., 2008, 2010). The four structural proteins, spike (S), envelope (E), membrane (M) and nucleocapsid (N), are encoded by subgenomic mRNAs. In addition, several putative nonstructural proteins, such as 3a, 3b, 6, 7a, 7b, 8a, 8b, 9b, are also encoded by subgenomic mRNAs (Snijder et al., 2003; Thiel et al., 2003).

Coronavirus N protein contains multiple functional domains. Sequence comparisons and structural studies have identified three main structural domains, although their primary sequence conservation is low (Lai and Cavanagh, 1997; Li et al., 2005). Of this the middle domain is an RNA-binding domain, capable of binding both coronavirus- and non-coronavirus-derived RNA sequences in vitro (Stohlman et al., 1988; Tan et al., 2012; Zhou et al., 1996). The motifs for ribosome binding and nucleolar localization signals have been assigned to domain III (Wurm et al., 2001). More recently, Chang et al. (2009) proposed that all coronavirus N proteins may share a similar modular organization. In cells expressing the N protein, it localizes either to the cytoplasm alone or to the cytoplasm and nucleolus (Hiscox et al., 2001). This nucleolar localization has been shown to be a common feature of the coronavirus family (Wurm et al., 2001). The prime function of the protein is to associate with the genomic RNA to form a ribonucleoprotein complex (RNP) and viral core (Davies et al., 1981; Escors et al., 2001; Narayana et al., 2000; Riso et al., 1996). The protein may also play an important role in the replication of the genomic RNA (Chang and Brian, 1996), and in the transcription and translation of subgenomic RNAs (sgRNA) (Almazán et al., 2004; Baric et al., 1988; Stohlman et al., 1988; Tahara et al., 1994; Zúñiga et al., 2010). In addition, N protein might inhibit host cell proliferation or delay cell growth, possibly by disrupting cytokinesis (Chen et al., 2002; Wurm et al., 2001). It can also stimulate strong humoral and cellular immune response, making it a potential vaccine candidate (Kim et al., 2004).

Coronaviruse N protein is an extensively phosphorylated and highly basic protein. It varies from 377 to 455 amino acids in length and has high serine content (7–11%) as potential targets for phosphorylation. This protein contains several basic amino

* Corresponding author. Fax: +65 67913856.
E-mail address: dxliu@ntu.edu.sg (D.X. Liu).
[1] Equal contributors.

0042-6822/$ - see front matter © 2013 Elsevier Inc. All rights reserved.
http://dx.doi.org/10.1016/j.virol.2013.06.014

acid-rich regions functioning as nucleolar localization signals and RNA-binding motifs, and a serine/arginine (S/R) rich motif (Li et al., 2005, Fan et al., 2005; Tan et al., 2006). Biochemical characterization and mutagenesis studies demonstrated that coronavirus N protein was also posttranslationally modified by covalent attachment to the small ubiquitin-like modifier (SUMO). Sumoylation may play a role in the self-association and homo-oligomerization of the N protein, and its interference of host cell division (Li et al., 2005).

Infectious Bronchitis Virus (IBV), a prototype coronavirus, is the etiological agent of infectious bronchitis, which impairs the respiratory and urogenital tracts of chickens (Cavanagh, 2007). Similar to other coronaviruses, IBV N protein is heavily phosphorylated. By using mass spectroscopic analysis, two conserved amino acid clusters, Ser190Ser192 and Thr378Ser379, in IBV N protein were identified as the two regions for phosphorylation (Chen et al., 2005). Subsequently, a total of six residues (Ser162, Ser170, Thr177, Ser389, Ser424 and Thr428) were identified as phosphorylation sites for mouse hepatitis virus (MHV) A59 N protein (White et al., 2007), and four phosphoserines at positions 9, 156, 254 and 256 were identified in transmissible gastroenteritis virus (TGEV) N protein (Calvo et al., 2005). In addition, the host cell kinase (s) responsible for phosphorylation of coronavirus N protein is beginning to emerge. One example is glycogen synthase kinase-3, which was shown to be involved in regulation of the phosphorylation of severe acute respiratory syndrome coronavirus (SARS-CoV) N protein (Wu et al., 2009). Current evidence suggests that phosphorylation may play important roles in regulation of the functions of coronavirus N protein. These included regulation of its subcellular location, viral RNA transcription, particle assembly, immunoreactivity and specificity (Calvo et al., 2005; Jayaram et al., 2005; Shin et al., 2007; Surjit et al., 2005; Spencer et al., 2008). However, the functional relevance of N protein phosphorylation has not been rigorously tested in the context of virus-infected cells using an infectious clone system, and host cell kinases responsible for phosphorylation of other coronavirus N proteins are not reported.

IBV infection perturbs cell cycle progression and arrests cell at the S and G2/M phases (Li et al., 2007; Wilson and Rangasamy, 2001; Wurm et al., 2001). More recently, IBV infection was shown to induce DNA damage response and activation of the ataxia-telangiectasia mutated (ATM) and Rad3-related (ATR) kinase/checkpoint kinase-1 (Chk1) pathway partly through interaction between coronavirus nsp13 and DNA polymerase delta (Pol δ) (Xu et al., 2011). In this study, we show that phosphorylation at the Thr378 and Ser379 sites is dependent on ATR, a kinase activated during IBV replication. Introduction of Ala substitutions at these two sites individually, in combination of the two, and together with the other two sites (Ser190 and Ser192), into an infectious IBV clone did not affect the recovery of recombinant viruses containing the mutations. A mutant virus (rIBV-Nm4) carrying Ala substitutions at all the four previously identified sites grew at a similar, if not better, growth rate as wild type virus. This study reveals a cellular kinase responsible for phosphorylation of a coronavirus N protein at two sites and the functional consequence of this modification on coronavirus replication in virus-infected cells.

Results

Specific recognition of IBV N protein by phosphorylated Chk1 antibodies in IBV-infected cells

In a previous study, we showed the phosphorylation of a number of ATR-specific substrates, including Chk1, the best studied ATR substrate on Ser317 and Ser345, and replication protein A2 (RPA2), a component of the heterotrimeric RPA complex, on Ser4/8 in IBV-infected cells (Xu et al., 2011). The specific residues for the ATM kinase activity including Chk2 on Thr68 and ATM on Ser1981, however, were not detected in the same infected cells, demonstrating the activation of the ATR–Chk1 pathway during IBV infection (Xu et al., 2011). During this study, we noted that, when cells were infected with IBV at high multiplicity of infection and an excess amount of samples was loaded, a batch of pChk1-specific antibodies was also able to detect clearly a band migrating slightly more rapidly than pChk1 in IBV-infected cells, but not in cells infected with the ultraviolet (UV)-inactivated IBV at 8 and 12 h post-infection (Fig. 1). It should be pointed out that this observation was not consistently made when pChk1-specific antibodies from different sources were used. It was also noted that apparently more pChk1 was detected in cells treated with UV-inactivated IBV (Fig. 1). This increased detection of pChk1 may represent cellular contamination from the inoculums, as the virus stocks used for UV irradiation were prepared by freezing/thawing the infected cells and were not purified.

Re-probing of the same membrane with antibodies against IBV N protein detected the N protein at the exact position (Fig. 1). This result suggests that the protein band detected by anti-pChk1 may be a phosphorylated form of the IBV N protein.

ATR-dependent phosphorylation of IBV N protein

A series of experiments was then carried out to confirm if this indeed represents a phosphorylated form of IBV N protein and if ATR is responsible for its phosphorylation. First, cells infected with IBV were analyzed by Western blot with antibodies against IBV N protein and ATM/ATR substrates. As shown in Fig. 2a, the full-length 48-kDa IBV N protein and several smaller bands, representing either premature or cleavage products derived from N protein (Li et al., 2005), were detected by Western blot with anti-IBV N antibodies. The 48-kDa band was also detected efficiently by the anti-ATM/ATR substrate antibodies (Fig. 2a). In addition, a background band with unknown identity was also detected from both mock- and IBV-infected cells by this antibody (Fig. 2a).

The involvement of ATR in the phosphorylation of IBV N protein was then analyzed by addition of 10 and 15 μM of Schisandrin B (SchB), a specific ATR inhibitor functioning in IBV-infected cells as demonstrated in a previous study (Xu et al., 2011), to IBV-infected

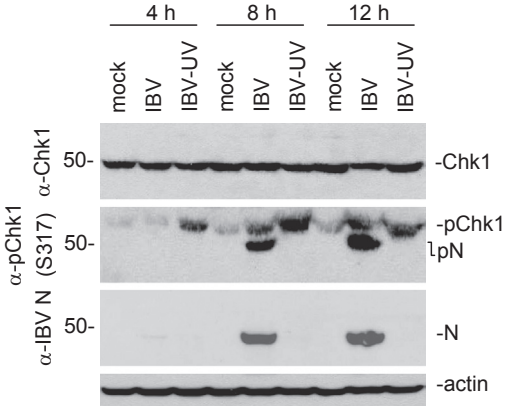

Fig. 1. Detection of phosphorylated IBV N protein by Western blot analysis with anti-phosphor Chk1(S317) antibodies. H1299 cells were infected with live IBV (IBV) or UV inactivated IBV (IBV-UV) at a multiplicity of infection of approximately 2. The mock-treated cells were also included as a control. At 4, 8 and 12 h post-infection, cells were harvested and total lysates were subjected to immunoblotting assay. The levels of phosphor-Chk1 (pChk1(S317)), total Chk1, actin and IBV N were determined with appropriate antibodies. Actin serves as a loading control, and IBV N protein as a marker of IBV infection.

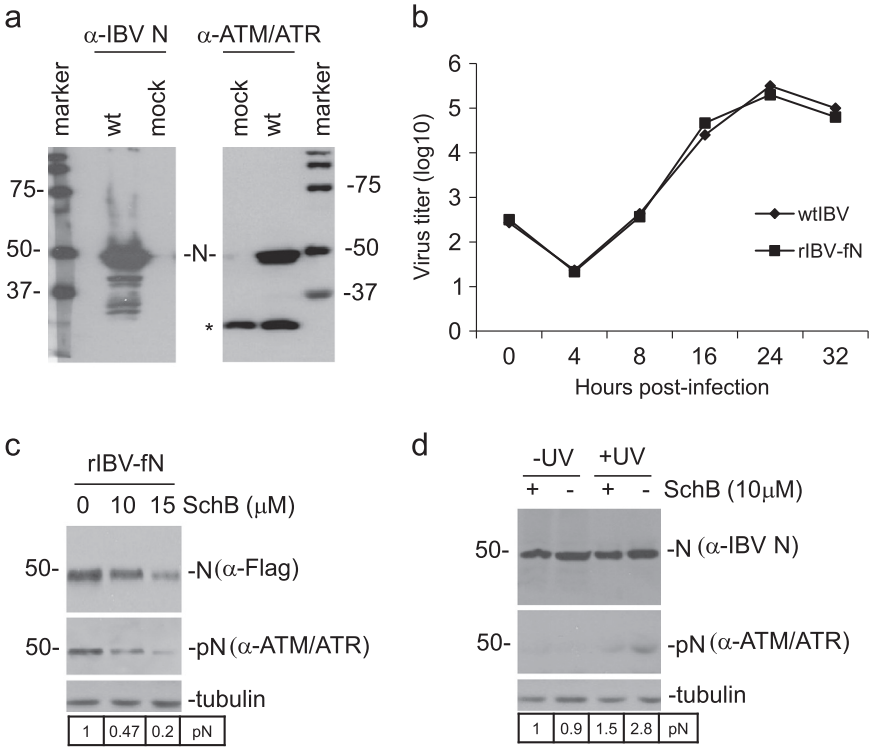

Fig. 2. Phosphorylation of IBV N protein by the activated ATR. (a) Detection of phosphorylated IBV N protein by Western blot analysis with anti-ATR/ATM substrate antibodies. H1299 cells were infected with IBV (wt) at a multiplicity of infection of approximately 1. The mock-treated cells were also included as a control. At 24 hours post-infection, cells were harvested and total lysates were subjected to immunoblotting assay. The levels of phosphorylated and total IBV N were determined with appropriate antibodies. (b) Analysis of the growth kinetics of wild type and rIBV-fN viruses. Monolayers of H1299 cells were infected with the viruses and harvested at 0, 4, 8, 16, 24 and 32 h post-inoculation. Viral stocks were prepared by freezing/thawing of the cells three times and TCID50 of each viral stock was determined by infecting five wells of Vero cells on 96-well plates in triplicate with 10-fold serial dilution of each viral stock. (c) Inhibition of ATR-dependent phosphorylation of IBV N protein by SchB in IBV-infected cells. H1299 cells were infected with rIBV-fN at a multiplicity of infection of approximately 1. At 4 h post-infection, 10 and 15 μM of SchB were added to the cultured media. Cells were harvested at 24 h post-infection and total lysates were subjected to immunoblotting assay. The levels of phosphorylated and total IBV N were determined with anti-Flag and anti-ATR/ATR substrates antibodies, respectively. Tubulin was included as a loading control. (d) Inhibition of ATR-dependent phosphorylation of IBV N protein by SchB in cells over-expressing the protein. H1299 cells were transfected with IBN N. At 22 h post-transfection, 10 μM of SchB was added to the culture media and cells were subjected to UV irradiation. Cells were harvested at 24 h post-infection and total lysates were subjected to immunoblotting assay. The levels of phosphorylated and total IBV N were determined with anti-IBV N and anti-ATR/ATR substrates antibodies, respectively. Tubulin was included as a loading control.

cells at 4 h post-infection. To more specifically analyze the full-length IBV N with an unrelated antibody, a recombinant IBV (rIBV-fN) with a Flag tag added to the N-terminus of the IBV N protein was constructed and used in this study. The recombinant virus showed very similar growth kinetics as wild type IBV (Fig. 2b). The cells were harvested at 24 h post-infection and analyzed by Western blot. As observed in our previous study (Xu et al., 2011), SchB exhibited a certain level of inhibitory effect on IBV replication. IBV N protein was reduced to 78% and 55% when 10 and 15 μM, respectively, of SchB were added, as revealed by Western blot using anti-Flag antibodies and densitometry analyses (Fig. 2c). Probing of the same membrane with antibodies against ATM/ATR substrates detected much less phosphorylated N protein in the presence of SchB (Fig. 2c). Quantification of the band intensities by densitometry after normalizing to the total N protein showed that the ATR-dependent phosphorylation of N protein was reduced to 47% and 2% after addition of 10 and 15 μM of SchB, respectively (Fig. 2c).

The phosphorylation of IBV N protein by ATR was then analyzed in cells overexpressing the N protein. Cells transfected with IBV N construct were subjected to UV irradiation at 22 h post-transfection in the presence or absence of 10 μM of SchB. Western blot analysis with antibodies against IBN N and ATM/ATR substrates showed that significantly less phosphorylated IBV N protein was detected in the UV-irradiated, transfected cells in the presence of 10 μM of SchB (Fig. 2d). In the absence of 10 μM of SchB, a 2.8-fold increase of the ATR-dependent phosphorylation of N protein was detected in the transfected cells after UV-irradiation, compared to that in the cells without UV-irradiation (Fig. 2d). In the presence of 10 μM of SchB, a 1.5-fold increase of the ATR-dependent phosphorylation of N protein was detected by the same comparison (Fig. 2d). These results would lend more support to the conclusion that ATR is one of the kinases responsible for phosphorylation of IBV N protein.

Construction and recovery of recombinant IBV carrying Ala substitutions at six predicted and previously identified phosphorylation sites on IBV N protein

To systematically map the ATR-dependent phosphorylation of IBV N protein, Ala substitutions at the four previously identified sites (Ser190, Ser192, Thr378 and Ser379) as well as two potential new sites (Ser65 and Thr109) predicted to be ATR substrates (Fig. 3a) were carried out. The Ala substitutions were then introduced into an IBV infectious clone either individually, or in combination of two, four, five or six, and nine recombinant IBVs were recovered from these constructs (Fig. 3a). All the nine mutant viruses were passaged in cells up to eight passages and their genetic stability was determined by nucleotide sequencing of the entire N protein-coding region. The sequencing results confirmed that the Ala substitutions were stably maintained in all the mutant viruses, and no additional mutations were introduced into the N protein during passaging. The growth properties of the recombinant viruses (passage 8) were then determined. As shown in Fig. 3b, very similar growth kinetics was found between wild type IBV and the mutant viruses. One notable

difference was that all mutant viruses reached their peak titers at 32 h post-infection, while wild type virus reached the peak titer at 24 h post-infection (Fig. 3b).

Mapping of the ATR-dependent phosphorylation sites on IBV N protein by Ala substitutions

Wild type and seven mutant viruses (Nm1–7, passage 3) were first used to infect H1299 cells. Total cell lysates were prepared and analyzed by Western blot with antibodies against ATM/ATR substrates. The results showed that the ATR-dependent phosphorylation of N protein was detected only in cells infected with wild type, Nm1 and Nm2 mutant viruses (Fig. 4a). The same band was not detected in cells infected with other five mutant viruses (Nm3–Nm7) (Fig. 4a). As all these five mutant viruses contain Ala substitutions at Thr378 and Ser379 positions, it suggests that phosphorylation of IBV N protein at these two sites is ATR-dependent. Re-probing of the same membrane with pChk1-specific antibodies detected a much reduced amount of the phosphorylated N protein in cells infected with Nm4 mutant virus, and moderately reduced amounts of the phosphorylated N protein in cells infected with Nm3, Nm5, Nm6 and Nm7 mutant viruses, respectively (Fig. 4a).

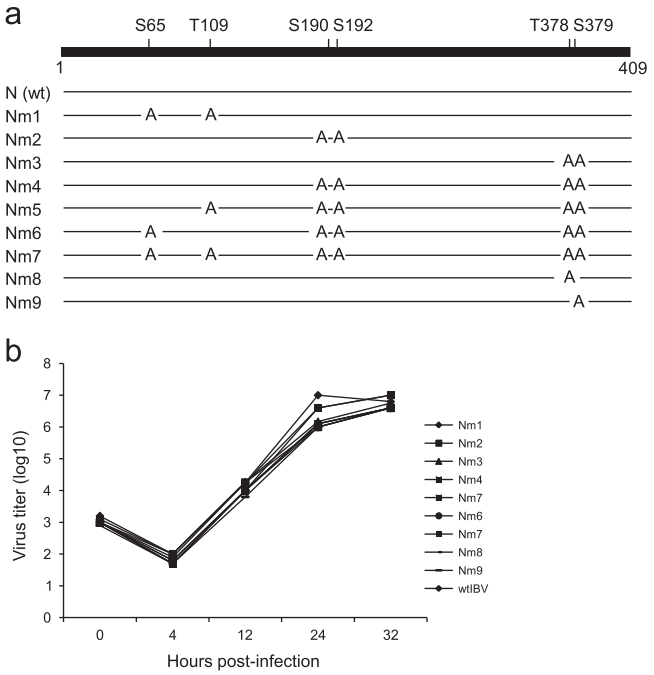

Fig. 3. Construction and recovery of mutant IBV carrying Ala substitutions at the predicted and previously identified phosphorylation sites on IBV N protein. (a) Diagram showing the positions of the four previously identified phosphorylation sites and two additional putative sites for ATR on IBV N protein. The Ala substitutions in each mutant construct are shown. (b) Analysis of the growth kinetics of wild type and the nine mutant viruses. Monolayers of H1299 cells were infected with the viruses and harvested at 0, 4, 12, 24 and 32 h post-infection. Viral stocks were prepared by freezing/thawing of the cells three times and TCID50 of each viral stock was determined by infecting five wells of Vero cells on 96-well plates with 10-fold serial dilution of each viral stock.

The additional two mutant viruses, Nm8 and Nm9 containing the Ala substitutions at Thr378 and Ser379, respectively (Fig. 3a), were then used to assess the relative contribution of the two residues to the ATR-dependent phosphorylation of IBV N protein. H1299 cells were infected with wild type, Nm3, Nm8 and Nm9 mutant viruses, and total cell lysates were prepared. Western blot analysis of total cell lysates with antibodies against ATM/ATR substrates showed, once again, detection of the ATR-dependent phosphorylation of IBV N protein in cells infected with the virus (Fig. 4b). No obvious phosphorylation of IBV N protein was detected by the same antiserum in cells infected with the three mutant viruses (Fig. 4b). These results indicate that both amino acid residues are phosphorylated by ATR and the neighboring sequence may affect this ATR-dependent phosphorylation of IBV N protein.

It was also noted that pChk1 was not readily detected by Western blot using both ATM/ATR substrate and pChk1-specific antibodies under the conditions shown in Fig. 4a and b. The reason may be due to the relatively low abundance of pChk1, compared to the phosphorylated N protein in virus-infected cells.

Characterization of IBVNm4 mutant virus carrying Ala substitutions at all the four previously identified phosphorylation sites on IBV N protein

The growth properties of IBVNm4 mutant virus were then characterized. For this purpose, Vero cells in duplicate were infected with wild type and IBVNm4 at a multiplicity of infection of approximately 1. At 24 h post-infection, one set of cells was stained

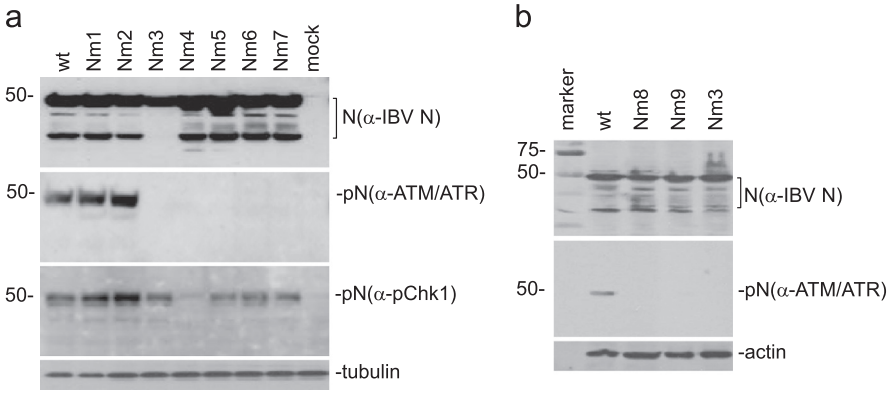

Fig. 4. Mapping of the ATR-dependent phosphorylation sites on IBV N protein. (a) The effects of Ala substitutions on the ATR-dependent phosphorylation of IBV N protein. H1299 cells were infected with wild type and seven mutant IBV (Nm1–Nm7) at a multiplicity of infection of approximately 1. The mock-treated cells were also included as a control. At 24 h post-infection, cells were harvested and total lysates were subjected to immunoblotting assay. The levels of ATR-dependent phosphorylated and total IBV N were determined with anti-IBV N, ATM/ATR substrates and pChk1-specific antibodies. Tubulin was included as a loading control. (b) Further analysis of the effects of Ala substitutions on the ATR-dependent phosphorylation of IBV N protein. H1299 cells were infected with wild type, Nm3, Nm8 and Nm9 mutant viruses at a multiplicity of infection of approximately 1. The mock-treated cells were also included as a control. At 24 h post-infection, cells were harvested and total lysates were subjected to immunoblotting assay. The levels of ATR-dependent phosphorylated and total IBV N were determined with anti-IBV N and anti-ATM/ATR substrates antibodies, respectively. Actin was included as a loading control.

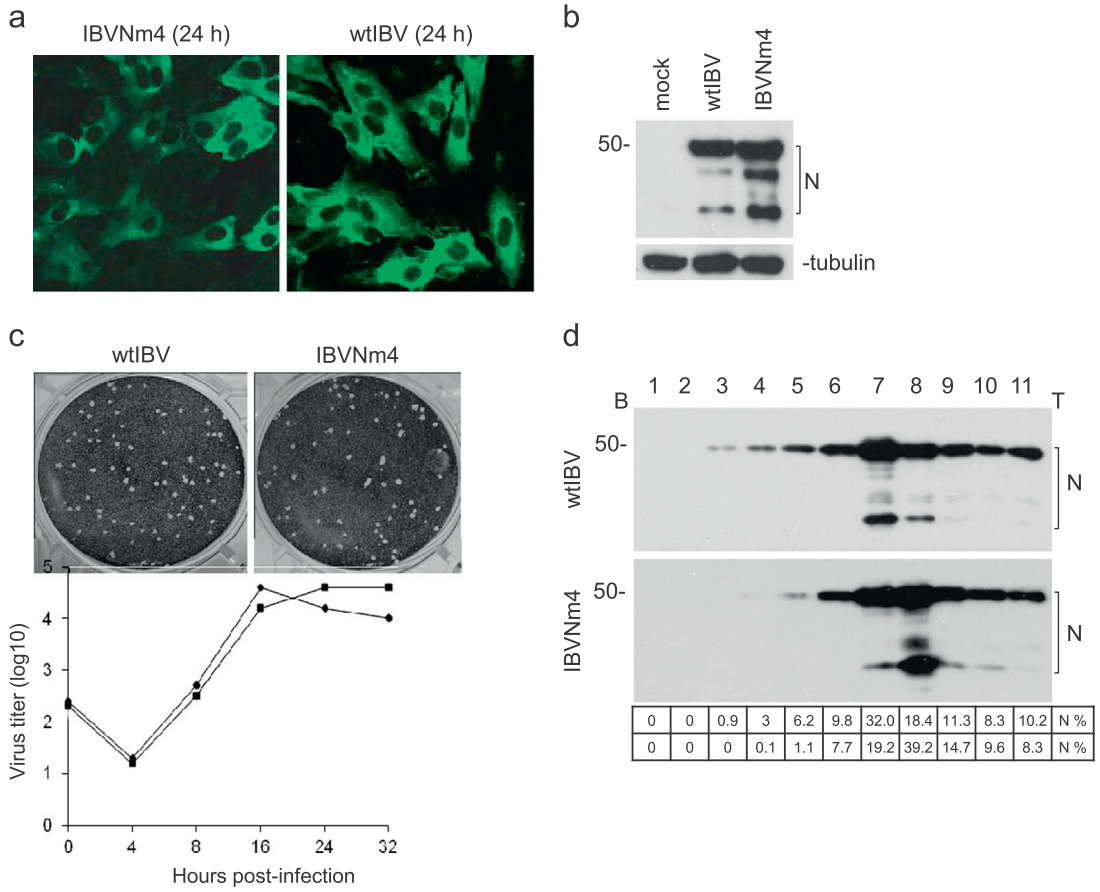

Fig. 5. Further characterization of the Nm4 mutant virus. (a) Immunofluoresent staining of Vero cells infected with wild type and Nm4 mutant virus. Vero cells were infected with wild type and Nm4 mutant viruses at a multiplicity of infection of approximately 1. At 24 h post-infection, cells were fixed and stained with anti-IBV N antibodies. (b) Western blot analysis of IBV N protein in cells infected with wild type and IBVNm4 mutant. Vero cells were infected with wild type and Nm4 mutant viruses at a multiplicity of infection of approximately 1. At 24 h post-infection, cells were harvested and total lysates were subjected to immunoblotting assay. The levels of total IBV N were determined with anti-IBV N antibodies. Tubulin was included as a loading control. (c) Analysis of the growth properties of wild type and Nm4 mutant viruses. Monolayers of Vero cells on a 6-well plate were infected with 100 μl of 1000-fold diluted virus stock and cultured in the presence of 0.5% carboxymethy cellulose at 37 °C for 3 days. The infected cells were fixed and stained with 0.1% toluidine (upper panels). To determine the growth curves of wild type and mutant IBV, Vero cells were infected with the viruses and harvested at 0, 4, 8, 16, 24, 36 h post-infection. Viral stocks were prepared by freezing/thawing of the cells three times and TCID50 of each viral stock was determined by infecting five wells of Vero cells on 96-well plates in triplicate with 10-fold serial dilution of each viral stock. (d) Analysis of wild type and Nm4 mutant viruses by ultracentrifugation in a 10–50% sucrose gradient. Vero cells were infected with wild type and Nm4 mutant viruses, at a multiplicity of infection of approximately 1. At 24 h post-infection, the cultured media were collected and cell debris was removed by centrifugation at 10,000 rpm for 10 min. The virus particles were pelleted through a 20% sucrose cushion. The pellets were resuspended in 1 ml medium and subjected to ultracentrifugation in a 10–50% linear sucrose gradient. Eleven fractions were collected and the presence of virus particles in each fraction was analyzed by Western blot with antibodies against IBV N protein. The percentage of virus in each fraction was calculated after determination of the amount of N protein in each fraction by densitometry.

by immunofluorescence with antibodies against IBV N protein. As shown in Fig. 4a, massive syncytium formation was observed in cells infected with both wild type and mutant viruses. No distinguishable difference in syncytium formation and subcellular distribution of N protein between wild type and the mutant viruses was observed (Fig. 5a). Western blot analysis of another set of the infected cells with anti-IBV N antibodies showed the presence of both full-length and other processed forms of the N protein (Li et al., 2005) (Fig. 5b). Interestingly, slightly more N protein was detected from cells infected with the mutant virus at this time point (Fig. 5b).

The growth properties of the mutant virus were then studied by plaque formation and growth kinetics studies. As shown in Fig. 5c, plaques with similar sizes were found in cells infected with both wild type and IBVNm4 mutant viruses at 24 h post-infection. Analysis of the growth kinetics of wild type and the mutant viruses also showed very similar growth properties for both viruses, although the mutant virus reached its peak titers at 24 h post-infection, which was 8 h later than did wild type virus (Fig. 5c). Interestingly, the mutant virus remained at peak titers until the end of the time course at 32 h post-infection (Fig. 5c). It is not clear if this may represent an altered cellular response to the infection caused by this mutant virus.

The buoyant density of IBVNm4 mutant virus was then analyzed by ultracentrifugation using 10–50% sucrose gradients, after collection of the virus from culture supernatants by spinning down through a 20% sucrose cushion. Eleven fractions were collected and analyzed by Western blot with antibodies against IBV N protein, which was used as a marker for the presence of virus particles. Both wild type and mutant viral particles were found to be present mainly in fractions 7 and 8 (50.4% for wild type and 58.4% for IBVNm4) (Fig. 5d). It was noted that more viral particles (32.0%) were found in fraction 7 for wild type IBV, but more virus particles (39.2%) were found in fraction 8 for the mutant virus (Fig. 5d). These results demonstrate that the mutant virus may have a slightly lower buoyant density than wild type virus. Further study would be required to confirm if this difference may reflect the difference in the phosphorylation of the N protein.

Discussion

Coronavirus N protein plays multiple functions during the viral replication cycle. Available evidence suggests that most of its

functions may be regulated by the phosphorylation of the protein (Calvo et al., 2005; Jayaram et al., 2005; Shin et al., 2007; Surjit et al., 2005; Spencer et al., 2008). In this study, two previously identified phosphorylation sites in IBV N protein, Thr378 and Ser379, are shown to be phosphorylated by ATR, which is activated by IBV-induced DNA replication stress during IBV infection of cells (Xu et al., 2011). Ala substitutions of these two residues together with the other two previously identified phosphorylation sites (Ser190 and Ser192) as well as two predicted sites for ATR individually or in combination did not affect the recovery of infectious viruses containing the mutations.

In this study, we provided evidence suggesting that phosphorylation of IBV N protein at Thr378 and Ser379 by ATR appears to play a limited, if any, regulatory function in IBV replication and infectivity in cultured cells. As IBVNm4 also covers Ala substitutions at other two previously identified phosphorylation sites (Ser190Ser192), it would point to the possibility that phosphorylation of coronavirus N protein at these four sites may represent a by-effect of host response to virus infection. Coronavirus infection may activate a diversity of host cell signal transduction pathways as well as kinases, which would in turn lead to the phosphorylation of viral N protein. This may explain why more phosphorylated N protein is incorporated into IBV virions (Jayaram et al., 2005), as extensive phosphorylation of N protein would occur at a relatively late stage of the viral infection cycle. It is currently unclear if this is specific to IBV, as some other coronaviruses, such as MHV, tend to incorporate hypophosphorylated N protein into virions (White et al., 2007)

On the other hand, we cannot rule out the possibility that phosphorylation of IBV N protein may occur at other positions in cells infected with Nm4 and other related mutant viruses, and phosphorylation at these alternate sites would functionally compensate for the loss of phosphorylation at these four positions. This possibility would be supported by the observation that significantly more phosphorylated N protein was detected in cells infected with Nm5, Nm6 and Nm7 mutant viruses, than in cells infected with Nm4. It appears that additional Ala substitutions at Ser65 and Thr109 in these three mutant viruses might induce more phosphorylation of IBV N protein at a site(s) recognized by the pChk1-specific antibodies used. In this context, it would be interesting to determine which phosphorylation site(s) of IBV N protein may be recognized by this pChk1-speific antiserum. Data present in this study are inconclusive, but appear to indicate that both Thr378 and Ser379 may be recognized specifically or non-specifically by the pChk1 antibodies used, as significantly reduced amounts of the phosphorylated N protein were detected in cells infected with mutant viruses containing mutations at these two positions, compared to that in cells infected with wild type and other mutants. However, as certain amounts of the phosphorylated N protein were still detected by this antiserum in cells infected with these mutant viruses, other phosphorylation site (s) must exist.

Multiple cellular kinases are involved in phosphorylation of coronavirus N protein. This may constitute another layer of regulatory mechanisms controlling the phosphorylation status of coronavirus N protein in virus-infected cells. For example, both Thr378 and Ser379 residues could be phosphorylated by casein kinase II (CKII), as predicted by computer-aided programs. It was reported that CKII can be stabilized by ATR-dependent phosphorylation of Chk1 at Ser317 in response to stalled DNA replication (Martin and Ouchi, 2008). This in turn would lead to phosphorylation of phosphatase and tensin homolog protein (PTEN) at Thr383. As IBV infection activates the ATR/Chk1 pathway, phosphorylation of IBV N protein at multiple sites may be also regulated by a similar mechanism. In addition, phosphorylation of N protein is most likely a dynamic process, timely regulated during the infection cycle. In this study, we showed that the phosphorylated N protein was detected by a pChk1-specific antibody at as early as 8 h post-infection, as well as at 24 h post-infection. Analysis of the effects of Ala substitutions on the phosphorylation status of IBV N protein in virus-infected cells was carried out at 24 h post-infection in most of the studies shown here. This time point was chosen based on the consideration that slightly delayed growth kinetics was observed in most of the mutant viruses. It was noted that more phosphorylated N protein was detected in cells infected with some mutant viruses (mainly Nm1 and Nm2 mutant viruses) than that in cells infected with wild type virus. This may reflect this dynamic regulatory process at this time point.

The successful recovery of viruses from all the mutant constructs confirms that phosphorylation at these positions is not essential for the viability of IBV in cultured cells. In fact, Western blot analysis of viral protein expression and viral growth kinetics analysis showed that most of the mutant viruses grew similarly well as wild type virus. This is confirmed by detailed analysis of the growth properties and kinetics of IBVNm4, showing that the mutant virus grew equally well, if not better, as wild type virus, although a slightly delayed growth kinetics was observed. Interestingly, after reaching peak titer at 24 h post-infection, the mutant virus remains at its peak titer until the end of the time course at 32 h post-infection. This is in contrast to wild type virus, which reached the peak titer at 16–24 h post-infection. The titers were gradually declined afterward. The underlying mechanisms for this difference are currently unknown, but it may reflect the difference in virus–host interactions between wild type and the mutant virus. One possibility is that the mutant virus may have an altered ability to induce cell death or cell cycle arrest. A more thorough study would be required to understand this issue more.

In conclusion, this study has provided strong evidence that activation of ATR/Chk1 pathway during IBV infection is responsible for phosphorylation of IBV N protein at two previously identified sites. Phosphorylation of N protein at these two positions, however, may play limited, if any, regulatory functions in IBV replication and infectivity in cultured cells. This would meanwhile reinforce our previous conclusion that IBV infection leads to efficient activation of the ATR pathway (Xu et al., 2011).

Materials and methods

Cells and viruses

Vero (ATCC CCL-81) cells were maintained in DMEM supplemented with 10% fetal bovine serum (FBS), penicillin (100 units/ml) and streptomycin (100 μg/ml) at 37 °C in a 5% CO_2 environment. H1299 (ATCC CRL-5803) cells were maintained in complete RPMI 1640 medium (JRH) supplemented with 10% newborn calf serum. Both Vero and H1299 cells were routinely used to culture Vero-adapted IBV (Liu et al., 1995, 1998; Tay et al., 2012)

The passage 65 (p65, designated wild type virus (wtIBV) of Vero-adapted IBV Beaudette was described before (Fang et al., 2005, 2007). The IBV strains were propagated in Vero cells and the tissue culture infective dose ($TCID_{50}$) of viral stocks was calculated by the Reed–Muench method (Yamada and Liu, 2009). Viral stocks were kept at −80 °C until use.

Chemicals and antibodies

Schisandrin B (SchB, Shanghai TauTo Biotech Co. LTD., China) was dissolved in DMSO and stored at −80 °C, as previously described (Xu et al., 2011).

Antibodies against Chk1Ser317 and phospho-(Ser/Thr) ATM/ATR substrates were purchased from Cell Signaling Technology

(Beverely, MA, USA). Antibody against Flag was from Sigma-Aldrich, and antibodies against actin and tubulin were from Santa Cruz (Santa Cruz, CA). Polyclonal antibodies against IBV N and S were raised in rabbits (Xu et al., 2010; Yamada and Liu, 2009). Horseradish peroxidase (HRP)-linked goat anti-rabbit secondary antibodies, HRP-linked goat anti-mouse secondary antibodies were purchased from Dako (Glostrup, Denmark).

Drug treatment and Luciferase reporter assay

Inhibitors SchB was added to cells 1 h prior to infection or 8 h post-transfection, and kept in the media during the infection. Cells of 90–95% confluency grown on 12-well plates were infected with IBV at a multiplicity of infectivity of approximately 1, and were harvested at the indicated time points post-infection.

Plasmid construction and transfection

Plasmid pKT-0 which has T7 promoter for transcription was used for transient transfection using the vaccinia/T7 recombinant virus (Ng and Liu, 2000, 2002). The pKT-N construct that encoded full-length N protein was previously reported (Li et al., 2005). Epitope-tagged constructs were made by overlap PCR and cloned into the pKT-0. Point mutations were made by site-directed mutagenesis using the Quikchange™ kit (Stratagene). Cells at about 90% confluency were infected with the recombinant vaccinia/T7 virus for 1 h followed by transfection of plasmid DNA using the Effectene Transfection reagent (Qiagen).

Western Blotting (WB)

Each sample was lysed with 1 × SDS sample loading buffer without bromophenol blue and the protein concentration was determined by the Bio-rad Protein Assay kit. Equal amounts of total protein were separated by SDS-PAGE and transferred to PVDF membranes. Membranes were incubated with a primary antibody, subsequently with HRP-conjugated secondary antibody, and detected using the ECL Advance Western Blotting Detection Kit (Amersham).

Immunofluorescent (IF) staining

Vero cells were cultivated in 4-well chamber slides (Iwaki). IBV-infected cells were washed with phosphate buffered saline (PBS) supplemented with 10% normal goat serum, fixed with 4% paraformaldehyde in PBS for 15 min, and permeabilized with 0.2% Triton X-100 for 10 min. IF staining was performed by incubating cells with polyclonal antibodies against IBV N protein and subsequently with the FITC-conjugated anti-rabbit IgG. Cells were examined by fluorescent microscopy.

Construction of mutant IBV by in vitro transcription of full-length wild type or mutant IBV cDNA and electroporation

The detailed procedure to create a full-length IBV cDNA clone was previously reported (Tan et al., 2006; Fang et al., 2007). The region of the IBV cDNA covering the N gene was replaced with mutant N genes, and subsequently ligated into full-length IBV cDNA. Full-length transcripts were generated in vitro using the mMessage mMachine T7 kit (Ambion, Austin, Tex). Wild type IBV N gene transcripts were also generated to enhance the recovery of virus. Vero cells at about 90% confluency were trypsinized, washed twice with ice-cold PBS, and resuspended in PBS. RNA transcripts were introduced into Vero cell by using the Bio-Rad Gene Pulser II electroporator. Cells were cultured overnight in 1% FBS-containing DMEM in a 6-well plate and further incubated in DMEM without FBS. At 48 h post-electroporation, viral RNA replication was investigated by RT-PCR of the negative strand gRNA. Transcription of subgenomic mRNAs was investigated by RT-PCR as described before (Tan et al., 2006; Fang et al., 2007). The N gene of recovered rIBV clones (at the 3rd passage in Vero cells) was amplified by RT-PCR and subsequently confirmed by the DNA sequencing analysis. Characterization was carried out with the 3rd passage of viruses in Vero cells.

Densitometry

The intensities of RNA and protein bands were quantified using ImageJ program according to the manufacturer's instruction.

Acknowledgement

This work was partially supported by a Competitive Research Programme (CRP) grant (R-154-000-529-281), the National Research Foundation, Singapore.

References

Almazán, F., Galán, C., Enjuanes, L., 2004. The nucleoprotein is required for efficient coronavirus genome replication. J. Virol. 78, 12683–12688.
Baric, R.S., Nelson, G.W., Fleming, J.O., Deans, R.J., Keck, J.G., Casteel, N., Stohlman, S.A., 1988. Interactions between coronavirus nucleocapsid protein and viral RNAs: implications for viral transcription. J. Virol. 62, 4280–4287.
Calvo, E., Escors, D., López, J.A., González, J.M., Alvarez, A., Arza, E., Enjuanes, L., 2005. Phosphorylation and subcellular localization of transmissible gastroenteritis virus nucleocapsid protein in infected cells. J. Gen. Virol. 86, 2255–2267.
Cavanagh, D., 2007. Coronavirus avian infectious bronchitis virus. Vet. Res. 38, 281–297.
Chang, C.K., Hsu, Y.L., Chang, Y.H., Chao, F.A., Wu, M.C., Huang, Y.S., Hu, C.K., Huang, T.H., 2009. Multiple nucleic acid binding sites and intrinsic disorder of severe acute respiratory syndrome coronavirus nucleocapsid protein: implications for ribonucleocapsid protein packaging. J. Virol. 83, 2255–2264.
Chang, R.Y., Brian, D.A., 1996. cis requirement for N-specific protein sequence in bovine coronavirus defective interfering RNA replication. J. Virol. 70, 2210–2217.
Chen, H., Gill, A., Dove, B.K., Emmett, S.R., Kemp, C.F., Ritchie, M.A., Dee, M., Hiscox, J.A., 2005. Mass spectroscopic characterization of the coronavirus infectious bronchitis virus nucleoprotein and elucidation of the role of phosphorylation in RNA binding by using surface plasmon resonance. J. Virol. 79 (2), 1164–1179.
Chen, H., Wurm, T., Britton, P., Brooks, G., Hiscox, J.A., 2002. Interaction of the coronavirus nucleocapsid with nucleolar antigens and the host cell. J. Virol. 76, 5233–5250.
Davies, H.A., Dourmashkin, R.R., MacNaughton, R., 1981. Ribonucleoprotein of avian infectious bronchitis virus. J. Gen. Virol. 53, 67–74.
Escors, D., Ortego, J., Laude, H., Enjuanes, L., 2001. The membrane M protein carboxy terminus binds to transmissible gastroenteritis coronavirus core and contributes to core stability. J. Virol. 75, 1312–1324.
Fan, H., Ooi, A., Tan, Y.W., Wang, S., Fang, S.G., Liu, D.X., Lescar., J., 2005. Crystal structure of the N-terminal domain from the nucleocapsid protein of coronavirus infectious bronchitis virus. Structure 13, 1859–1868.
Fang, S., Shen, H., Wang, J., Tay, F.P., Liu, D.X., 2010. Functional and genetic studies of the substrate specificity of coronavirus infectious bronchitis virus 3C-like proteinase. J. Virol. 84, 7325–7336.
Fang, S.G., Shen, H., Wang, J., Tay, F.P., Liu, D.X., 2008. Proteolytic processing of polyproteins 1a and 1ab between non-structural proteins 10 and 11/12 of Coronavirus infectious bronchitis virus is dispensable for viral replication in cultured cells. Virology 379, 175–180.
Fang, S.G., Chen, B., Tay, F.P., Ng, B.S., Liu., D.X., 2007. An arginine-to-proline mutation in a domain with undefined functions within the helicase protein (Nsp13) is lethal to the coronavirus infectious bronchitis virus in cultured cells. Virology 358, 136–147.
Fang, S.G., Shen, S., Tay, F.P., Liu., D.X., 2005. Selection of and recombination between minor variants lead to the adaptation of an avian coronavirus to primate cells. Biochem. Biophys. Res. Commun. 336, 417–423.
Hiscox, J.A., Wurm, T., Wilson, L., Cavanagh, D., Britton, P., Brooks, G., 2001. The coronavirus infectious bronchitis virus nucleoprotein localizes to the nucleolus. J. Virol. 75, 506–512.
Jayaram, J., Youn, S., Collisson, E.W., 2005. The virion N protein of infectious bronchitis virus is more phosphorylated than the N protein from infected cell lysates. Virology 339, 127–135.
Kim, T.W., Lee, J.H., Hung, C.F., Peng, S., Roden, R., Wang, M.C., Viscidi, R., Tsai, Y.C., He, L., Chen, P.P., Boyd, D.A.K., Wu, T.C., 2004. Generation and characterization of DNA vaccines targeting the nucleocapsid protein of severe acute respiratory syndrome coronavirus. J. Virol. 78, 4638–4645.

Lai, M.M., Cavanagh, D., 1997. The molecular biology of coronaviruses. Adv. Virus Res. 48, 1–100.
Li, F.Q., Xiao, H., Tam, J.P., Liu, D.X., 2005. Sumoylation of the nucleocapsid protein of severe acute respiratory syndrome associated coronavirus. FEBS Lett. 579, 2387–2396.
Li, Q., Tam, J.P., Liu., D.X., 2007. Cell cycle arrest and apoptosis induced by the coronavirus infectious bronchitis virus in the absence of p53. Virology 365, 435–445.
Liu, D.X., Tibbles, K.W., Cavanagh, D., Brown, T.D., Brierley, I., 1995. Identification, expression, and processing of an 87-kDa polypeptide encoded by ORF 1a of the coronavirus infectious bronchitis virus. Virology 208, 48–57.
Liu, D.X., Shen, S., Xu, H.Y., Wang, S.F., 1998. Proteolytic mapping of the coronavirus infectious bronchitis virus 1b polyprotein: evidence for the presence of four cleavage sites of the 3C-like proteinase and identification of two novel cleavage products. Virology 246, 288–297.
Martin, S.A., Ouchi, T., 2008. Cellular commitment to reentry into the cell cycle after stalled DNA is determined by site-specific phosphorylation of Chk1 and PTEN. Mol. Cancer Ther. 7, 2509–2516.
Narayana, K., Maeda, A., Maeda, J., Makina, S., 2000. Characterization of the coronavirus M protein and nuclocapsid interaction in infected cells. J. Virol. 74, 8127–8134.
Ng, L.F.P., Liu, D.X., 2000. Further characterization of the coronavirus infectious bronchitis virus 3C-like proteinase and determination of a new cleavage site. Virology 272, 27–39.
Ng, L.F., Liu, D.X., 2002. Membrane association and dimerization of a cysteine-rich, 16-kilodalton polypeptide released from the C-terminal region of the coronavirus infectious bronchitis virus 1a polyprotein. J. Virol. 76, 6257–6267.
Riso, C., Anton, I.M., Enjuanes, L., Carrascosa, J.L., 1996. The transmissible gastroenteritis coronavirus contains a spherical core shell consisting of M and N proteins. J. Virol. 70, 4773–4777.
Shin, G.C., Chung, Y.S., Kim, I.S., Cho, H.W., Kang, C., 2007. Antigenic characterization of severe acute respiratory syndrome-coronavirus nucleocapsid protein expressed in insect cells: the effect of phosphorylation on immunoreactivity and specificity. Virus Res. 127 (1), 71–80.
Snijder, E.J., Bredenbeek, P.J., Dobbe, J.C., Thiel, V., Ziebuhr, J., Poon, L.L.M., Guan, Y., Rozanov, M., Spaan, W.J.M., Gorbalenya, A.E., 2003. Unique and Conserved features of genome and proteome of SARS-coronavirus, an early split-off from the coronavirus group 2 lineage. J. Mol. Biol. 331, 991–1004.
Spencer, K.A., Dee, M., Britton, P., Hiscox, J.A., 2008. Role of phosphorylation clusters in the biology of the coronavirus infectious bronchitis virus nucleocapsid protein. Virology 370 (2), 373–381.
Stohlman, S.A., Baric, R.S., Nelson, G.W., Soe, L.H., Welter, L.M., Deans, R.J., 1988. Specific interaction between coronavirus leader RNA and nucleocapsid protein. J. Virol. 62, 4288–4295.
Surjit, M., Kumar, R., Mishra, R.N., Reddy, M.K., Chow, V.T., Lal, S.K., 2005. The severe acute respiratory syndrome coronavirus nucleocapsid protein is phosphorylated and localizes in the cytoplasm by 14-3-3-mediated translocation. J. Virol. 79 (17), 11476–11486.
Tahara, S.M., Dietlin, T.A, Bergmann, C.C., Nelson, G.W., Kyuwa, S., Anthony, R.P., Stohlman, S.A., 1994. Coronavirus translational regulation: leader affects mRNA efficiency. Virology 202, 621–630.
Tan, Y.W., Fang, S.G., Fan, H., Lescar, J., Liu., D.X., 2006. Amino acid residues critical for RNA-binding in the N-terminal domain of the nucleocapsid protein are essential determinants for the replication and infectivity of coronavirus in cultured cells. Nucleic Acids Res. 34, 4816–4825.
Tan, Y.W., Hong, W., Liu., D.X., 2012. Binding of the 5′-untranslated region of coronavirus RNA to zinc finger CCHC-type and RNA binding motif 1 enhances viral replication and transcription. Nucleic Acids Res. 40, 5065–5077.
Thiel, V., Ivanov, K.A., Putics, A., Hertzig, T., Schelle, B., Bayer, S., Weissbrich, B., Snijder, E.J., Rabenau, H., Doerr, H.W., Gorbalenya, A.E., Ziebuhr, J., 2003. Mechanisms and enzymes involved in SARS coronavirus genome expression. J. Gen. Virol. 84, 2305–2315.
Tay, F.P., Huang, M., Wang, L., Yamada, Y., Liu, D.X., 2012. Characterization of cellular furin content as a potential factor determining the susceptibility of cultured human and animal cells to coronavirus infectious bronchitis virus infection. Virology 433, 421–430.
White, T.C., Yi, Z., Hogue, B.G., 2007. Identification of mouse hepatitis coronavirus A59 nucleocapsid protein phosphorylation sites. Virus Res. 126 (1–2), 139–148.
Wilson, V.G., Rangasamy, D., 2001. Viral interaction with the host cell sumoylation system. Virus Res. 81, 17–27.
Wu, C.H., Yeh, S.H., Tsay, Y.G., Shieh, Y.H., Kao, C.L., Chen, Y.S., Wang, S.H., Kuo, T.J., Chen, D.S., Chen, P.J., 2009. Glycogen synthase kinase-3 regulates the phosphorylation of severe acute respiratory syndrome coronavirus nucleocapsid protein and viral replication. J. Biol. Chem. 284, 5229–5239.
Wurm, T., Chen, H., Britton, P., Brooks, G., Hiscox, J.A., 2001. Localization to the nucleolus is a common feature of coronavirus nucleoproteins and the protein may disrupt host cell division. J. Virol. 75, 9345–9356.
Xu, L.H., Huang, M., Fang, S.G., Liu., D.X., 2011. Coronavirus Infection Induces DNA replication stress partly through interaction of its nonstructural protein 13 with the p125 subunit of DNA polymerase delta. J. Biol. Chem. 286, 39546–39559.
Xu, L.H., Khadijah, S., Fang, S.G., Wang, L., Tay, F.P.L., Liu., D.X., 2010. The cellular RNA helicase DDX1 interacts with coronavirus nonstructural protein 14 and enhances viral replication. J. Virol. 84, 8571–8583.
Yamada, Y., Liu, D.X., 2009. Proteolytic activation of the spike protein at a novel RRRR/S motif is implicated in furin-dependent entry, syncytium formation and infectivity of coronavirus infectious bronchitis virus in cultured cells. J. Virol. 83, 8744–8758.
Zhou, M., Williams, A.K., Chung, S.I., Wang, L., Collisson, E.W., 1996. The infectious bronchitis virus nucleocapsid protein binds RNA sequences in the 3′ terminus of the genome. Virology 217, 191–199.
Zúñiga, S., Cruz, J.L., Sola, I., Mateos-Gómez, P.A., Palacio, L., Enjuanes, L., 2010. Coronavirus nucleocapsid protein facilitates template switching and is required for efficient transcription. J. Virol. 84, 2169–2175.